Penerbit Akademia Baru

Journal of Advanced Research in Fluid Mechanics and Thermal Sciences

Journal homepage: www.akademiabaru.com/arfmts.html
ISSN: 2289-7879

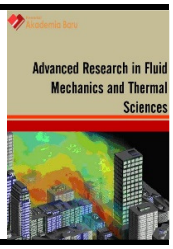

Effects of Air-Induced Duct Diameter on Flow and Heat Transfer Characteristics of Multiple Impinging Jets

Open Access

Kirttayoth Yeranee[1], Makatar Wae-hayee[1,*], Yu Rao[2], Chayut Nuntadusit[1]

[1] Department of Mechanical Engineering, Faculty of Engineering, Prince of Songkla University, 90112 Hat Yai, Songkhla, Thailand
[2] School of Mechanical Engineering, Shanghai Jiao Tong University, 200240, Shanghai, China

ARTICLE INFO

Article history:
Received 30 September 2018
Received in revised form 8 November 2018
Accepted 9 November 2018
Available online 15 November 2018

ABSTRACT

The objective of this study is to investigate effects of air-induced duct diameter on flow and heat transfer of multiple impingement jet, experimentally and numerically. 5 columns x 5 rows of pipe nozzles, which have diameter of d=17.2 mm, was arranged with inline configuration. The diameter of air-induced duct (D) were varied at D/d=2, 4 and 6, and Reynolds numbers was fixed at Re=30,000. Moreover, the jet-to-plate distances (H) were studied at H/d=6 and H/d=8, respectively. Nusselt number was calculated by measuring temperature distributions on the surface using infrared camera. Numerical study was performed to visualize the flow characteristics and to elucidate the heat transfer mechanism. The results showed that the highest average Nusselt number was found at D/d=4 with short jet-to-plate distance, H/d=6.

Keywords:
Multiple impinging jets, Heat transfer enhancement, Air-induce duct, CFD

1. Introduction

Jet impingement is applied to heat and cool rapidly the target surface due to high heat and mass transfer rates at the stagnation region. This technique is thus used widely in thermal engineering industrial processes, such as the tempering of glass process, the annealing of metal, the drying of textiles, and the cooling of gas turbine vanes. In the case of a single jet, many researchers have found that the characteristics or the rate of heat transfer on a target surface depend on mass flow rates, a jet-to-plate distance and nozzle shapes. Generally, the maximum heat transfer is found at the end of the potential core in the range of 2 to 6 times of nozzle diameter from jet outlet [1-8].

In the case of multiple impinging jet, however, the interference of adjacent jets before impinging on the surface and the jet fountain after impinging are also affected to its heat transfer. The interference of adjacent jets is particularly stronger when the jet-to-plate distance is higher and the jet-to-jet spacing is narrower. In contrast, the jet fountain from the collision of wall jets is stronger when the jet-to-plate distance becomes shorter and the jet-to-jet spacing becomes larger [1 and 9-12].

* *Corresponding author.*
E-mail address: wmakatar@eng.psu.ac.th (Makatar Wae-hayee)

For all cases of impinging jet, there are two principal factors governing heat transfer rate of impinging jets: (1) momentum of jet impinging on the wall, and (2) turbulent intensity of jet before impinging. Momentum of jets could be greater by increasing the power of pump or blower, while the method to increase turbulent intensity could be classified depending on external power requirement into two methods: active and passive methods. Active method uses external source to increase mass flow rate, which also enhance momentum of jet, but passive method requires no external power. Passive methods are thus studied intensely by many researchers, such as attaching of triangular tabs [13] or mesh screen [14] at the nozzle outlets; inserting swirling tape [15-19] in to the nozzle; or modifying the nozzle geometry [7,8,20].

Mounting expansion pipe or air-induced duct at jet exits is one of the methods that enhance turbulent intensity since this would induce ambient fluid into jet flow, resulting in higher heat transfer on the surface [21-24]. An array of impinging jet mounting air-induced duct at the end of jet exit have been conducted by K. Yeranee *et al.,* [25]. They proved that this method could enhance heat transfer on the impingement surface. In addition, the simulation of jet flow has been demonstrated that for the case of mounting air-induced duct, ambient air was entrained into the jet flow greater than the case of conventional jet. The diameter of air-induced duct is envisioned to be one of parameters, which influence a heat transfer rate on the surface. Ambient air could be more entered the duct depending on a suction force due to the effect of diameter of the air-induced duct, and flow circulation after impingement can be blocked when the diameter of air-induced duct is larger. The diameter of air-induced duct is thus interesting to be further explored.

According to these evidences, the purpose of this study is to investigate the effect of the air-induced duct diameter on flow and heat transfer characteristics of the multiple jet, experimentally and numerically. Moreover, a jet-to-plate distance (H) were also examined to compare which condition having high heat transfer rate on the impingement surface.

2. Methodology

2.1 Experimental Model and Parameters

The experimental model of multiple impinging jet mounting air-induced duct is shown in Figure 1. Jet discharging from nozzle pipes, which impinged perpendicularly on the impingement surface, were arranged 5 rows × 5 columns with inline configuration. Air-induced ducts were mounted at the end of each nozzle outlet. A three-dimensional Cartesian coordinate system were located at the center of impinging surface. The axis line Z indicated along the axial of the jet; axis line X and Y were on the impingement surface normal to the jet.

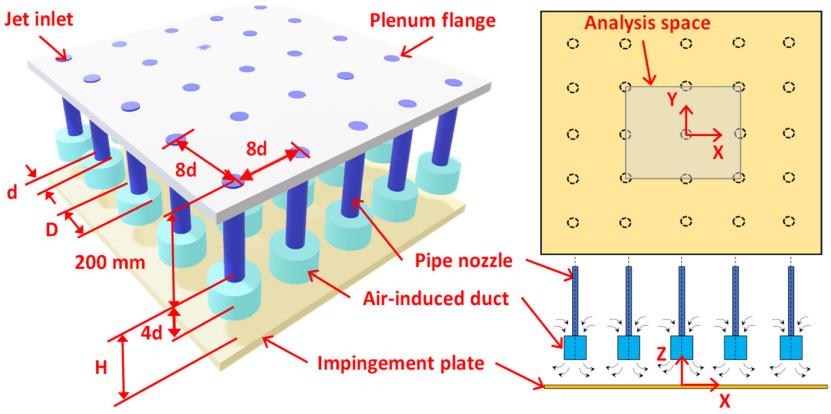

Fig. 1. Experimental model of multiple impinging jet mounting air-induced duct

The pipe nozzles have the inner diameter of 17.2 mm and the length of 200 mm, which was long enough to ensure that the fluid was fully developed flow. The inner diameter of air-induced was varied at D/d = 2, 4 and 6, and the length of the duct was fixed at 4 times of nozzle diameter (4d). A jet-to-jet spacing was fixed at S=8d, and Reynolds number was also kept constant at 30,000. The details of the experimental parameters were summarized in Table 1.

Table 1
The summery of the experimental parameters

Parameters	Variable
The inner diameter of air-induced duct	D/d = 2, 4 and 6
Jet-to-plate distance	H/d = 6 and 8
Jet-to-jet spacing	S/d= 8
Reynolds number	Re = 30,000

2.2 Experimental Apparatus

The diagram of the experimental apparatus is depicted in Figure 2. The air was accelerated passing orifice flow meter by blower, and entered a heater chamber, which equipped with heater. The air then passed though pressure chamber, which was attached with 3 layers of mesh screen to ensure that the temperature and the velocity of the air were uniform before reaching each nozzle pipe. The temperature of jet was set at 27.0°C by a power controller and a temperature controller, and the jet velocity was controlled at Re=30,000 by adjusting inverter.

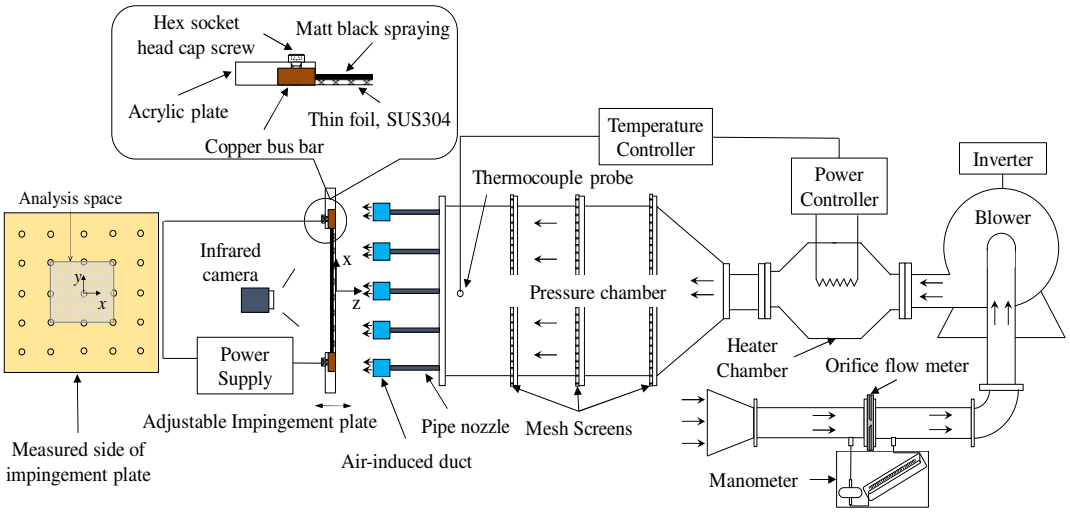

Fig. 2. Diagram of the experimental apparatus

The impingement plate can move in Z-axis direction to adjust the required jet-to-plate distance. The plate was made of acrylic plate, which was opened a rectangular hollow at its center. A very thin stainless-steel foil (0.03 mm in thickness) that was used for measuring the temperature on analysis space, which was stretched tightly on the rectangular hollow of the acrylic plate by two copper bus bars.

A power supply unit was used to applied direct current power to the copper bus bar for heating up the stainless-steel foil. Due to very thin of the foil thickness which can be treated the temperature on both sides being the same, the temperature distributions were captured on the opposite side to impingement surface using an infrared camera (FLIR, T420) [5, 8, 9 and 25]. The measured side was sprayed with matt black having emissivity of 0.95.

2.3 Heat Transfer Measurement

The model of heat transfer measurement is to heat the measured surface, then the surface is cooled by impinging jet with lower temperature. The local heat transfer coefficient, h, was calculated from Equation 1.

$$h = \frac{\dot{q}_{total}}{T_w - T_j} \quad (1)$$

where the total heat flux, $\dot{q}_{total}$, is heat dissipation from applying direct current which has been elaborated in our previous study [24-25]. T_w is the wall temperature with heat flux and T_j is the wall temperature without heat flux.

The local Nusselt number, Nu, and the average Nusselt number, $\overline{Nu}$, were evaluated using Equation 2 and Equation 3, respectively.

$$Nu = \frac{hd}{k} \quad (2)$$

$$\overline{Nu} = \frac{\bar{h}d}{k} \quad (3)$$

where the inner diameter of the pipe nozzle, d, the thermal conductivity of the jet, k and the average heat transfer coefficient from averaging wall temperature, $\bar{h}$.

3. Numerical Study

3.1 Numerical Model and Boundary Conditions

For demonstrating the flow patterns, the numerical study was computed using, CFD, ANSYS FLUENT (version 15.0). The numerical model and boundary conditions are shown in Figure 3. The dimensions of the numerical model were created with the same to experimental model one.

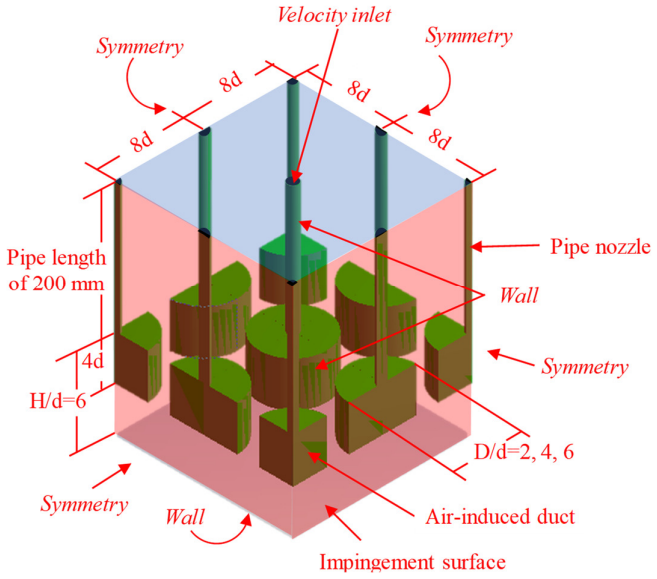

Fig. 3. Numerical model and boundary conditions

The numerical model could be divided in three section. The first section was the main pipe nozzles, having diameter of 17.2 mm and length of 200 mm. The second section represented the air-induced ducts, which have the length of 4 times of nozzle diameter, and the diameter of the duct (D) were varied at D/d=2, 4 and 6. The third section was concerned an impingement surface, so jet-to-plate distances (H) were fixed at H/d=6. The boundary conditions consisted of velocity inlet, wall and symmetry that were summarized the details of numerical model in Table 2.

Table 2
The details of boundary conditions

Selected surfaces	As define
Nozzles inlet	Velocity inlet, 27.21 m/s
Front and Side surface	Symmetry
Top, Bottom, nozzle pipe surface and the duct surface	Wall

3.2 Grid System and Validation

The grid distribution of the numerical model is represented in Figure 4. In this model, the rectangular grid was generated mainly, and the triangular grid was created properly to fill in circle region, such as nozzle pipe zones and air-induced duct regions. For the zone near impingement surface that had very high velocity gradient, the grids were finely controlled. To achieve an accurate solution, the number of grid was modified until the dimensionless wall distances being approximately 1 (y^+≈1) [26]. y^+ was calculated from Equation 4.

$$y^+ = \frac{y_1 u_\tau}{v} \tag{4}$$

where shear velocity, u_τ, the distance to the nearest wall, y_1 and the kinematic viscosity of air, v.

The influences of grid quantities on y^+distributions on the impingement surface of middle jet (Y/d=0, X/d=0) in the range of -2.0≤X/d≤2.0 are represented in Figure 5(a). The number of grids making the y^+≈1 had two sets, including 2,982,080 and 3,541,220 cells. Therefore, the grid at 2,982,080 elements was selected for applying in numerical simulation in this work due to lower computational cost.

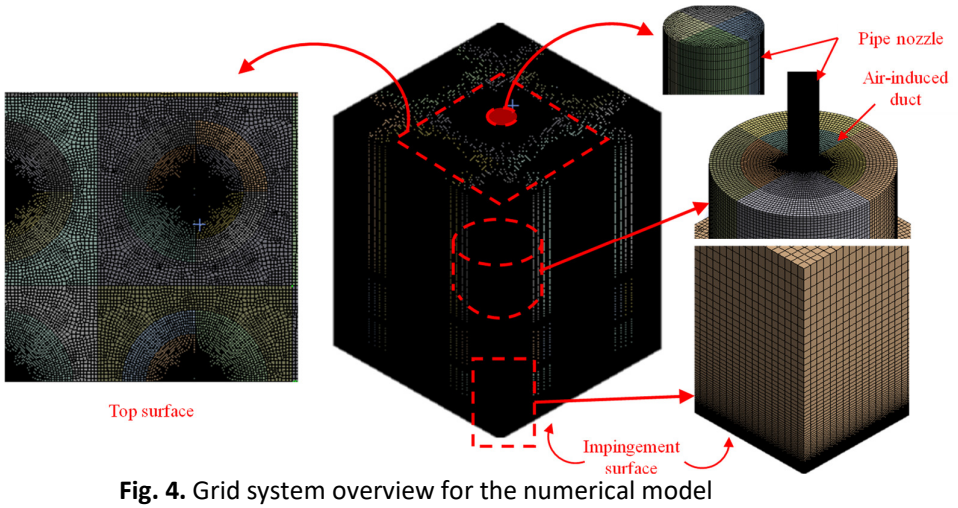

Fig. 4. Grid system overview for the numerical model

In order to validate simulation results, the jet velocity profiles at pipe outlet (-2.0≤X/d≤2.0) of middle jet (Y/d=0, X/d=0) from simulation and experiment results at H/d=6 were compared as shown in Figure 5 (b). The numerical results agreed with the experimental data. However, there was small discrepancy at the edge of nozzle pipe.

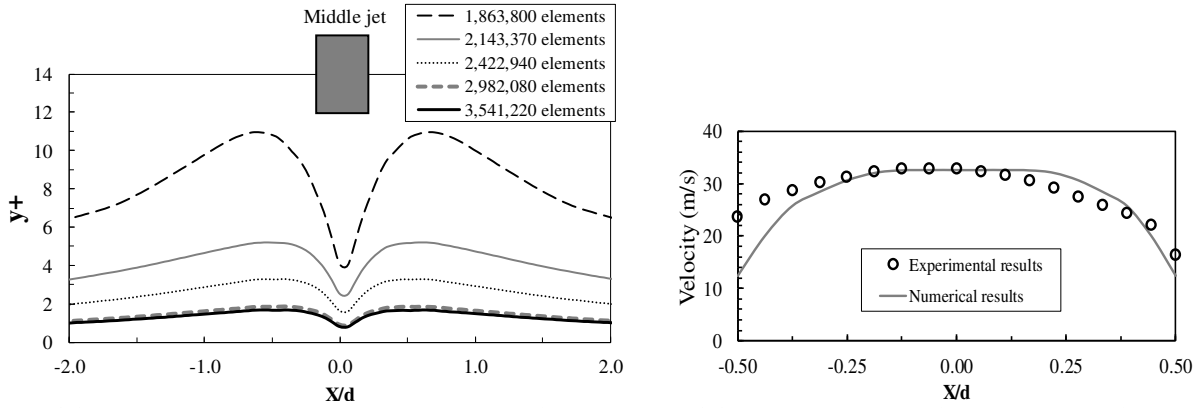

(a) y^+ distributions on the impingement surface (b) The comparison of jet velocity profiles

Fig. 5. The effects of grid dependency and CFD result validation for middle jet (Y/d=0, X/d=0) at H/d=6

3.3 Numerical Method

Computations were performed to solve Reynolds averaged continuity and Navier-Stokes equations under considering boundary conditions. The normal-velocity relaxation (v^2-f turbulence model) was applied to revel the flow characteristics since the numerical results were proved that agreed very well with experiments [27, 28]. It was highly recommended for solving the impinging problem with moderate computational cost by [29]. The SIMPLE scheme was selected to handle with pressure-velocity coupling, and the PRESTO algorithm was used to carry out the pressure discretization [30, 31]. The Second Order Upwind scheme was applied to deal with the rest of the spatial discretization. The iterative solution was insured to be converged when the residual of all the variables were less than 10^{-5}.

4. Results and Discussions

4.1 Flow Patterns

Velocity vectors on Z-X plane passing the middle pipe nozzle (Y/d=0) are shown in Figure 6. The circle marks shown in each figure represents the air entrainment at nozzle outlet for no. 1, the jet flow mixing with ambient air for no. 2, and stands for the area of accumulated jet after impingement for no. 3. In the case of conventional jet (Figure 6(a)), ambient air was induced initially by main jet flow at the nozzle outlet (Circle mark 1) and was mixed continuously with the main jet (Circle mark 2), causing velocity spread and decay. Wall jet interacted with each other after impingement at interval jet, which causing circulation flow turned back to the main jet flow (Circle mark 3).

In the latter cases with air-induced duct at D/d=2, 4 and 6 (Figure 6(b), (c) and (d)), the ambient air which was induced into the main jet is greater than the case of conventional jet (Figure 6(a)). It could be observed by the vectors in the duct being longer. Only for the case of D/d=2 (Figure 6(b)), the surrounding air was not further mixed with the main jet flow due to shielding by the duct. When the duct diameter was expanded at D/d=4 (Figure 6(c)), the entrainment air was more induced into the duct and then mixed with the main jet, so it caused to increase turbulence intensity of jet before impingement which will be discussed. For the biggest diameter of air-induced duct (D/d=6, Figure

10(d)), the duct was thus found to be able to induce ambient air being more than the others. The excessive entrainment air, which was not mixed with the jet flow, can impinge directly on the impingement surface, causing the stagnation area of jet being larger. In addition, with the largest diameter of air-induced duct (D/d=6, Figure 10(d)), flow characteristics of jet are similar to the case of conventional jet.

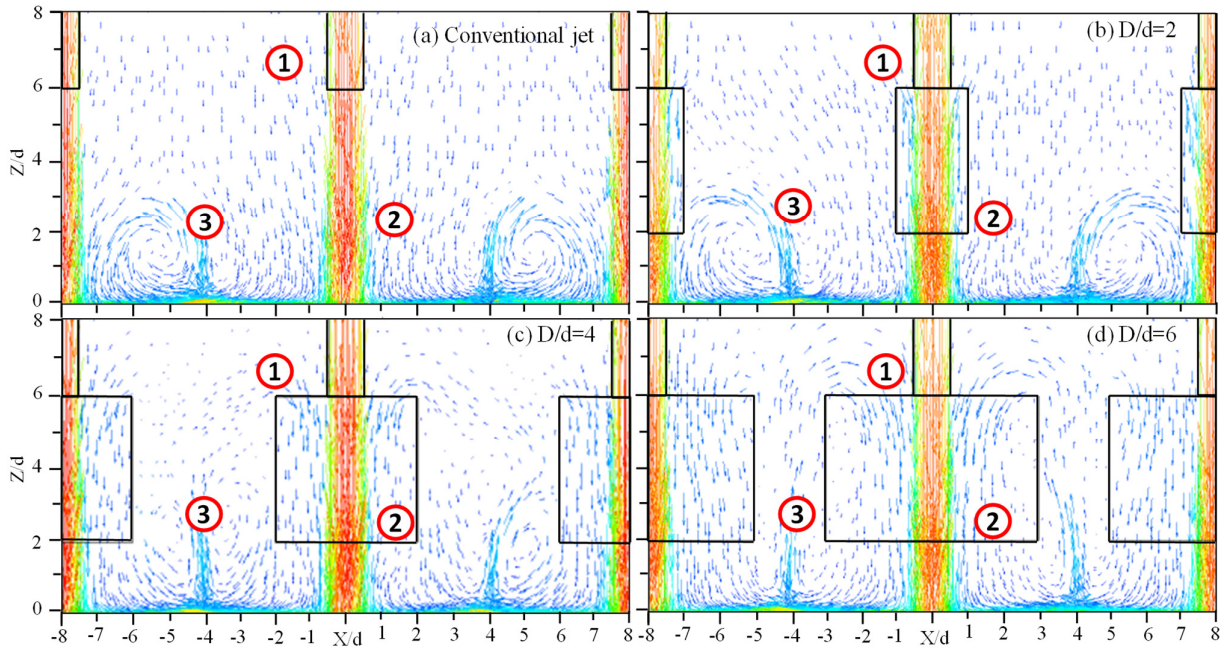

Fig. 6. Velocity vectors on Z-X plane, passing middle jets at Y/d=0, S/d=8, H/d=6 (CFD results, Re=30,000)

After the jet impinging on the surface, the circulation flow (No. 3 circle mark) became smaller when air-induced duct diameter was larger. Consequently, the circulation flow disappeared completely at the case of D/d=6 (Figure 6(d)) due to blocking by the duct.

From these phenomena, it was expected that heat transfer region had larger area when the duct was more expanded, but heat transfer at stagnation point was lesser when the duct diameter got too large.

TKE profiles in all cases of mounting air-induced duct were also found to be higher than the case of conventional jet. However, the larger duct did not lead to a high TKE as occurred in the velocity profile case, and the highest TKE was found in the case of D/d=4. The high TKE of induced air affects to strong turbulent intensity of jet that would affect to high heat transfer on the surface of impinging jet, which was mentioned in 'Introduction'. Therefore, the highest heat transfer could be found in the cases of D/d=4.

Figure 7 represents the velocity profiles (Figure 7(a)) and turbulence kinetic energy, TKE, profiles (Figure 7(b)) along X/d direction at middle jet outlet (Y/d=0, X/d=0). The region at X/d≤0.5 was for main jet flow, and the section in range of 0.5<X/d≤3 was for the area where ambient air entering the air-induced duct.

For all cases of mounting air-induced duct (D/d=2, 4 and 6), the velocity profiles in the duct region, 0.5<X/d≤1 for D/d=2, 0.5<X/d≤2 for D/d=4 and 0.5<X/d≤3 for D/d=6, were higher than the case of conventional jet. The highest velocity profile was found in the case of the smallest air-induced duct, D/d=2, yet it was just only in small range, 0.5≤X/d≤1. The velocity profiles tended to decrease when the duct was more expanded due to low suction force from diameter effect. However, the area where

ambient air entering the duct was larger, which was observed to be the largest in the case of D/d=6. It can be noticed that the volume of air was more induced when the diameter of the duct was enlarged.

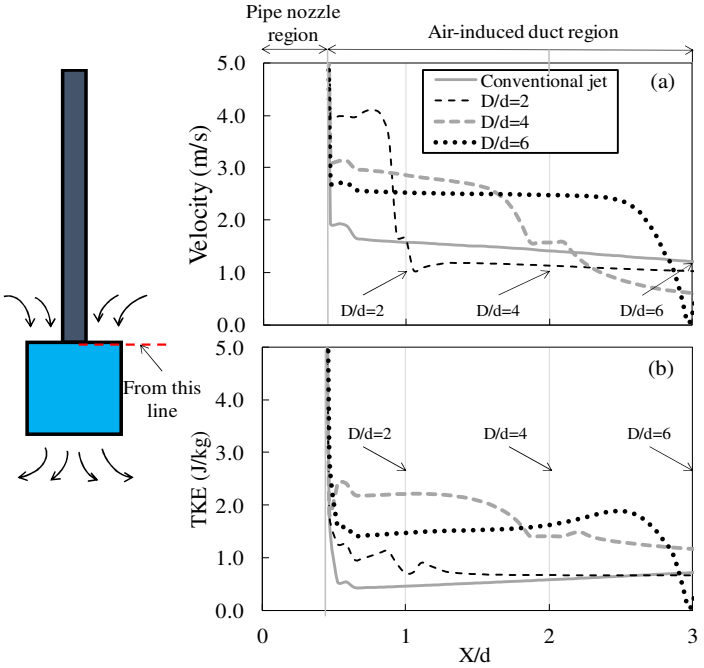

Fig. 7. (a) Velocity and (b) Turbulence Kinetic Energy profiles along Z-X direction at middle jet outlet 0≤X/d≤3 (CFD results, S/d=8, H/d=6, Re=30,000)

4.2 Nusselt Number Contour

The Nusselt number contours on the impingement surface at Re=30,000 are shown in Figure 8. The small circles in the figures indicated the pipe nozzle location, its location depending on the jet-to-jet spacing (S), and the bigger ones represented air-induced duct, which were concentric with each pipe nozzles, the size depending on its diameter. Nusselt number contours could be divided into three regions namely: (1) an area of high Nusselt number (Nu≥120) representing the stagnation region where a jet impinged directly to the surface, (2) an area of medium Nusselt number (90≤Nu≤120) showing the region around the stagnation zone, and (3) an area of low Nusselt number (Nu<90) indicating the jet interval region where spent jet vent out. Generally, the area of high and medium Nusselt number became smaller when the jet-to-plate distance (H) is higher. This result has been found similarly to many works [5, 9 and 24].

At a jet-to-plate distance H/d=6, the area of high Nusselt number was larger when diameter of air-induced duct was expanded, which agreed with flow characteristics in previous section, and the largest area of high Nusselt number was observed in the case of D/d=4 (Figure 8(c)). This could be explained that an entrainment air in the duct mixed with the jet flow, which enhance the turbulence intensity before impingement as earlier discussed in flow characteristics, resulting in high Nusselt number at stagnation region. When the diameter of the duct was too large, D/d=6 (Figure 8(d)), the area of high Nusselt number at stagnation region became smaller than the other cases. However, the areas of medium and low Nusselt number were comparable to the other cases.

For the cases of H/d=8, the area of high Nusselt number in the case of conventional jet was smaller than those cases of jet mounting air-induced duct. The results were similar to the cases of H/d=6 which area of high Nusselt number at stagnation region of jet with mounting air-induced duct (D/d=2 and 4, Figure 8 (f) and (g)) is larger than the case of conventional jet (Figure 8 (e)), but the area of high Nusselt number in the case of D/d=2 and 4 (Figure 8(f) and (g)) was comparable. It could be clarified that the diameter was more effective when apply to the case of short jet-to-plate distance (H/d=6).

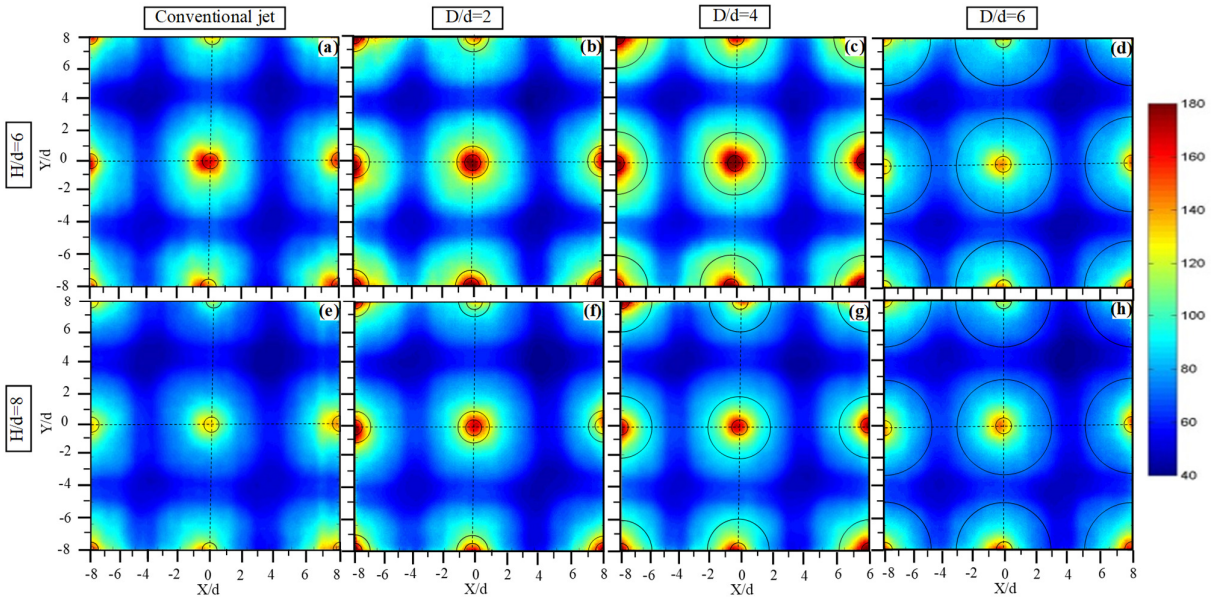

Fig. 8. Nusselt number contour on the impingement surface, Re=30,000 (Experimental results)

4.3 Local Nusselt Number

Figure 9 shows the distributions of local Nusselt number along the center of nozzles (Y/d=0). The rectangular symbols above the Figure represent the nozzle locations. For all cases, the peak of Nusselt number was found at the jet positions or impingement regions (X/d=-8, 0 and 8), and the trough of Nusselt number was observed at the jet interval (X/d=-4 and 4).

In the case of H/d=6 (Figure 9(a)), the peak of Nusselt number at stagnation point became higher when the duct was expanded, except for the case of D/d=6. The Nusselt number at jet interval was, however, comparable to all cases. For the cases of H/d=8 (Figure 9(b)), the peak of Nusselt number in the case of jet with air-induced duct was found to be higher than the case of conventional jet. For all cases of mounting the duct, the peak of Nusselt number and the trough of Nusselt number were similar. This show that the effect of mounting air-induced duct on an increase of Nusselt number in area of stagnation zone is greater that the area of jet interval.

4.4 Average Nusselt Number

Figure 10 represents the average Nusselt number on the impingement plate that was calculated using Equation 3 over the analysis space. The average Nusselt number for all cases of H/d=6 was generally higher than those of H/d=8 even though all cases of H/d=8 were mounted with air-induced duct.

As a result, the highest average Nusselt number was found remarkably in the case of jet mounting air-induced duct for shorter jet-to-plate distance (H/d=6) at D/d=4. Hence, it was cleare that a larger duct diameter can yield better heat transfer – up to limit (D/d=4), and this shows a 10.59% increase as compared to the case of conventional jet. For H/d=8, the average Nusselt number was also observed to be the highest at D/d=4, representing a 4.66% higher than the case of jet without duct. In short, the effect of mounting air-induced duct on heat transfer enhancement of impinging jets at H/d=6 is more effective than that at H/d=8.

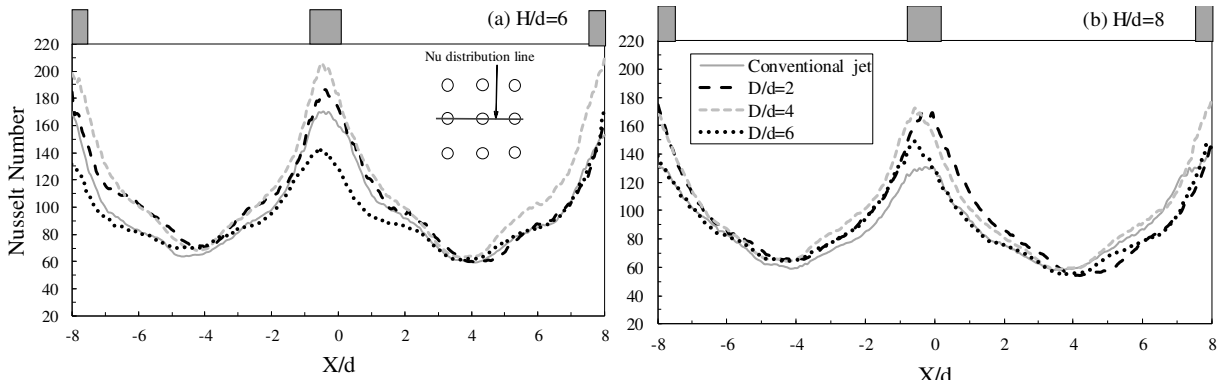

Fig. 9. The distributions of local Nusselt number along the center of nozzles (Y/d=0) (a) H/d=6 and (b) H/d=8, Re=30,000 (Experiment results)

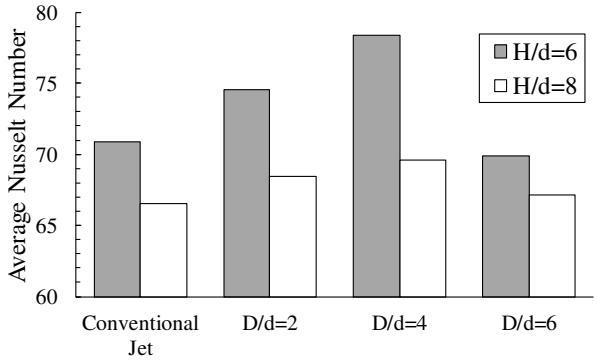

Fig. 10. The average Nusselt number on the impingement plate for the case of H/d=6 and H/d=8, (Experimental results, Re=30,000).

5. Conclusions

In this study, the effects of air-induced duct diameter on flow and heat transfer characteristics of impinging jets have been explored experimentally and numerically. The jet-to-plate distance was also investigated to seek the influence on heat transfer enhancement under assigned condition. Remarkable results can be summarized as followed:

1. Jets mounting air-induced duct could induce ambient air entraining into the jet flow greater than the case of conventional jet. At moderate duct diameter (D/d=4), a Turbulent Kinetic Energy (TKE) of entrainment air entering the duct was found to be higher than other cases.

2. Average Nusselt number of jet with mounting air-induced duct at D/d=4 was the highest. This coincided with the highest TKE of entrainment air entering the duct at D/d=4.

3. For short jet-to-plate distance (H/d=6), average Nusselt number was found to be higher than that of the larger jet-to-plate distance throughout air-induced duct diameters. Therefore, the effect

of mounting air-induced duct on heat transfer enhancement of impinging jets at H/d=6 is more effective than that at H/d=8.

Acknowledgement
This research was financially supported by the Thailand Research Fund (TRF), grant No. MGR5980082.

References

[1] Martin, H. "Heat and mass transfer between impinging gas jets and solid surfaces." *Advances in Heat Transfer* 13, (1977): 1-60.
[2] Jambunathan, K., Lai, E., Moss, M.A. and Button, L. "A review of heat transfer data for single circular jet impingement." *International Journal of Heat and Fluid Flow* 13, no. 2 (1992): 106-115.
[3] Viskanta, R. "Heat transfer to impinging isothermal gas and flame jets." *Experimental Thermal and Fluid Science* 6, no. 2 (1993): 111-134.
[4] Huber, A.M. and Viskanta, R. "Impingement heat transfer with a single rosette nozzle." *Experimental Thermal and Fluid Science* 9, no. 3 (1994): 320-329.
[5] Katti, V. and Prabhu, S.V. "Experimental study and theoretical analysis of local heat transfer distribution between smooth flat surface and impinging air jet from a circular straight pipe nozzle." *International Journal of Heat and Mass Transfer* 51, no. 17-18 (2008): 4480-4495.
[6] Guo, Q., Wen, Z. and Dou, R. "Experimental and numerical study on the transient heat-transfer characteristics of circular air-jet impingement on a flat plat." *International Journal of Heat and Mass Transfer* 104, (2017): 1177-1188.
[7] Dano, B.P.E., Liburdy, J.A. and Kanokjaruvijit, K. "Flow characteristics and heat transfer performances of a semi-confined impinging array of jets: effect of nozzle geometry." *International Journal of Heat and Mass Transfer* 48, no. 3-4 (2005): 691-701.
[8] Nuntadusit, C., Wae-hayee, M., Tekasakul, P. and Eiamsa-ard, S. "Local heat transfer characteristics of array impinging jets from elongated orifices." *International Communications in Heat and Mass Transfer* 39, no. 8 (2012): 1154-1164.
[9] Geers, L.F.G., Tummers, M.J., Bueninck, T.J. and Hanjalic, K. "Heat transfer correlation for hexagonal and in-line arrays of impinging jets." *International Journal of Heat and Mass Transfer* 51, no. 21-22 (2008): 5389-5399.
[10] San, J.Y. and Lai, M.D. "Optimum jet-to-jet spacing of heat transfer for staggered arrays of impinging air jets." *International Journal of Heat and Mass Transfer* 44, no. 21 (2001): 3997-4007.
[11] Huber, A.M. and Viskanta, R. "Effect of jet-to-jet spacing on convection heat transfer to confined, impinging arrays of axisymmetric air jets." *International Journal of Heat and Mass Transfer* 37, no. 18 (1997): 2859-2869.
[12] Hollworth, B.R., and Berry, R.D. "Heat transfer from arrays of impinging jets with large jet-to-jet spacing." *Journal of Heat Transfer* 100, no. 2 (1978): 352-357.
[13] Gao, N., Sun, H. and Ewing, D. "Heat transfer to impinging round jets with triangular tabs,." *International Journal of Heat and Mass Transfer* 46, no. 14 (2003): 2557-2569.
[14] Zhou, D.W. and Lee, S.J. "Heat transfer enhancement of impinging jets using mesh screens." *International Journal of Heat and Mass Transfer* 47, no. 11-12 (2004): 2097-2108.
[15] Wen, M.Y. and Jang, K.J. "An impingement cooling on a flat surface by using circular jet with longitudinal swirling strips." *International Journal of Heat and Mass Transfer* 46, no. 24 (2003): 4657-4667.
[16] Nuntadusit, C., Wae-hayee, M., Bunyajitradulya, A. and Eiamsa-ard, S. "Heat transfer enhancement by multiple swirling impinging jets with twisted-tape swirl generators." *International Communications in Heat and Mass Transfer* 39, no. 1 (2012): 102-107.
[17] Nuntadusit, C., Wae-hayee, M., Bunyajitradulya, A. and Eiamsa-ard, S. "Visualization of flow and heat transfer characteristics for swirling impinging jet." *International Communications in Heat and Mass Transfer* 39, no. 5 (2012) 640-648.
[18] Alekseenko, S.V, Bilsky, A.V., Dulin, V.M. and Markovich, D.M. "Experimental study of an impinging jet with different swirl rates." *International Journal of Heat and Mass Transfer* 28, no. 6 (2007): 1340-1359.
[19] Bakirci, K. and Bilen, K. "Visualization of heat transfer for impinging swirl flow." *Experimental Thermal and Fluid Science* 32, no. 1 (2007): 182-191.
[20] Colucci, D.W. and Viskanta, R. "Effect of nozzle geometry on local convective heat transfer to a confined impinging air jet." *Experimental Thermal and Fluid Science* 13, no. 1 (1996): 71-80.
[21] Zeng, Y., New, T.H. and Chng, T.L. "Flow behavior of turbulent nozzle jets issuing from beveled collars." *Experimental Thermal and Fluid Science* 35, no. 8 (2001): 1555-1564.

[22] Zeng, Y., New, T.H. and Tsai, H.M. "On the use of notched collars on an axisymmetric jet." *Experimental Thermal and Fluid Science* 33, no. 6 (2009): 1029-1034.
[23] Nathan, G.J., Mi, J., Alwahabi, Z.T., Newbold, G.J.R and Nobes, D.S. "Impacts of a jet's exit flow pattern on mixing and combustion performance." *Progress in Energy and Combustion Science* 32, no. 5-6 (2006): 496-538.
[24] Nuntadusit, C., Wae-hayee, M. and Keawchoothong, N. "Heat transfer enhancement on a surface of impinging jet by increasing entrainment using air-augmented duct." *International Journal of Heat and Mass Transfer* 127 (2018): 751-767.
[25] Yeranee, K., Wae-hayee, M., Piya, I., Rao, Y. and Nuntadusit, C. "The study of flow and heat transfer characteristics of impinging jet array mounting air-induced duct." *IOP Conference Series: Materials Science and Engineering* 243, no. 1 (2017).
[26] Olsson, E.E.M, Ahrne, L.M., Tragardh, A.C. "Flow and heat transfer from multiple slot air jets impinging on circular cylinders." *Journal of Food Engineering* 67 (2005): 273-280.
[27] Sunden, B., Larocque, J. and Wu, Z. "Numerical simulation of heat transfer from impinging swirling jets." In *Impingement Cooling in Gas Turbines: Design, Applications, And Limitations*, p. 185-203.
[28] Behnia, M., Parneix, S. and Durbin, P. A. "Prediction of heat transfer in an axisymmetric turbulent jet impinging on a flat plate." *International Journal of Heat and Mass Transfer* 41, no. 12 (1998): 1845-1855.
[29] Zuckerman, N. and Lior, N. "Jet impingement heat transfer: physics, correlations and numerical modeling." *Advances in Heat Transfer* 39, (2006): 565-631.
[30] Jehad, D.G., Hashim, G.A., Zarzoor, A.K., Nor Azwadi, C.S. "Numerical study of turbulent flow over backward-facing step with different turbelence models." *Journal of Advanced Research Design* 4, no. 1 (2015): 20-27.
[31] Jamil, M.M., Adamu, M.I., Ibrahim, T.R., Hashim, G.A. "Numerical study of separation length of flow through rectangular channel with baffle plantes." *Journal of Advanced Research Design* 7, no. 1 (2015): 19-33.